Applied Thermal Engineering, Volume 196, September 2021, Article number 117254
DOI: 10.1016/j.applthermaleng.2021.117254

Techno-economic-environmental assessment of biomass oxy-gasification staged oxy-combustion for negative emission combined heat and power

Navid Khallaghi [a,b], Harish Jeswani [b], Dawid P. Hanak [a,*], Vasilije Manovic [a,*]

[a] Energy and Power, School of Water, Energy and Environment,
Cranfield University,
Bedford, Bedfordshire, MK43 0AL, UK

[b] Department of Chemical Engineering and Analytical Science, University of Manchester, Manchester, M13 9PL, UK

Accepted by Applied Thermal Engineering, 117254
doi: doi.org/10.1016/j.applthermaleng.2021.117254

***Corresponding authors:** Dawid Hanak (d.p.hanak@cranfield.ac.uk);*

Vasilije Manovic (v.manovic@cranfield.ac.uk)

Abstract

Climate change mitigation requires developing low-carbon technologies capable of achieving CO_2 emission reductions at the gigatonne scale and affordable cost. Biomass gasification, coupled with carbon capture and storage, offers a direction to atmospheric CO_2 removal. To compensate for the issues associate with the high-investment requirement of CO_2 removal unit and lower efficiency compared to fossil-based power cycles, this study proposed a conceptual system for combined heat and power, based on biomass oxy-gasification integrated with staged oxy-combustion combined cycle (BOXS-CC). Aspen Plus® is used to develop the process model of the proposed cycle. The results obtained in the techno-economic analysis showed that the net power efficiency of the proposed concept with 50.2 kg/s biomass flowrate was 41.6%, and the heat efficiency was 27.4%, leading to a total efficiency of 69.0%, including CO_2 compression. Moreover, the economic assessment of BOXS-CC revealed that it can achieve a levelised cost of electricity of €21.4/MWh, considering

the heat and carbon prices of €46.5/MWh and €40/tCO_2, respectively. Such economic performance is superior compared to fossil fuel power plants without CO_2 capture. The environmental assessment shows that BOX-CC system results in net negative emissions of 766 kg CO_2 eq./MWh_e.

Keywords: Biomass gasification; oxy-combustion cycle; techno-economic analysis; combined heat and power; Greenhouse gas emissions

1. Introduction

Reaching the CO_2 emission reduction targets of the Paris Agreement to limit global warming below 2°C is unlikely to be met since energy consumption is currently growing by 2% per year, and this growth is highly dependent on fossil fuels [1]. Carbon capture and storage (CCS) is a cost-effective solution to limit greenhouse gas emissions [2]. If CCS was excluded from the decarbonisation scenario, the cost of achieving the emission reduction targets would increase by up to 140% due to the considerably higher costs of alternative decarbonisation pathways [3–5].

CCS is often associated with the decarbonisation of fossil fuel-based combustion systems. Yet, it can also be integrated with bio-energy conversion technologies and, similarly to direct air capture technologies, achieve negative CO_2 emissions [6]. Therefore, bio-energy with CCS (BECCS) is currently being regarded as a promising negative-emission technology that can help meet the CO_2 emission reduction targets by 2050 [7,8]. Among the thermochemical options for biomass conversion (direct combustion, torrefaction, pyrolysis, gasification and hydrothermal liquefaction), gasification is one of the most efficient options been widely applied for biomass conversion [9]. Several studies have been conducted on the integration of biomass gasification with CCS. Dinca et al. [10] performed a techno-economic analysis of biomass gasification power plant with amine-based CO_2 capture. The overall efficiency and levelised cost of electricity (LCOE) of the power plant were around 47% and £65/MWh, respectively. Zang et al. [11] performed a techno-economic comparison of different biomass integrated gasification combined cycles. They revealed that the electric efficiencies of the power plants with CCS vary between 23.9–27.1%, while their LCOE is in the range of 188–228 €/MWh. Xiang et al. [12] analysed the effect of the gasification temperature and pressure on the performance of the biomass integrated gasification combined cycle with oxy-fuel combustion. They revealed that the maximum electric efficiency of 35.4% is achievable at gasification temperature and pressure of 1000°C and 3.5 MPa, respectively.

Combined heat and power (CHP) systems achieve higher total efficiencies than the power generation systems by enabling the supply of electric power and hot water for district heating [13,14]. Few works can be found regarding the integration of biomass gasification with CHP. Perna et al. [15] investigated the effect of biomass gasification with CHP. They showed that the electric and total efficiencies for biomass gasification integrated with conventional combined cycle are 17.3% and 69.7%, respectively.

Pérez et al. [16] performed a techno-economic analysis on a lab-scale CHP system integrated with biomass gasification. They revealed that the system's net electric and total efficiencies are 23.4% and 55.8%, respectively, while the LCOE is £16.8/MWh.

Among all different kinds of gasifying agents (O_2, air, steam, CO_2, etc.), high-purity O_2 exploitation results in higher heating value syngas [17]. Yet, in this case, the air separation unit (ASU) operation is necessary that increases the capital cost of the plant [18], which is a disadvantage to its commercialisation. The concept of staged combustion has been applied to the natural gas-fired oxy-combustion combined cycle by Khallaghi et al. [19]. Such an oxy-combustion cycle was shown to have a comparable efficiency (51.2%) to the state-of-the-art NG-fired oxy-combustion cycles, such as the Allam cycle (55%) [20]. Importantly, due to its less complex layout and lower volumetric flow rates throughout the system, the levelised cost of electricity for the proposed cycle (£33/MWh) was shown to be competitive to that of the Allam cycle (£50/MWh) [18,21]. This was primarily due to lower capital cost, regardless of the net power efficiency being lower by 3%. Therefore, to compensate for the higher capital cost associated with biomass oxy-gasification, this work aims to evaluate the techno-economic feasibility of a biomass oxy-gasification integrated with a staged oxy-combustion combined cycle (BOXS-CC) for CHP generation with negative CO_2 emissions. Aspen Plus® is used to develop the process simulation and then, the effect of split fraction and gasification and combustion temperature on the cycle performance were investigated. Moreover, the results obtained from the optimal thermodynamic performance of the proposed cycle are used for economic feasibility evaluation of the BOXS-CC.

2. Process description and simulation

Figure 1 presents a schematic of the proposed BOXS-CC process. It is assumed that a complete conversion of biomass takes place in the presence of high-purity oxygen, generated in the ASU, as a gasifying agent, in a reactor (Gasifier). Syngas from the gasification consists mainly of H_2, N_2, CO, CO_2, CH_4, H_2S and H_2O; solid residues are removed in a separator. The syngas is then cooled down, and the extracted heat is utilised for district heating.

The acceptable level of H_2S is up to 8 ppm at the inlet of a gas turbine [22]. Therefore, H_2S removal with ZnO sorbent (Reaction R1), which is among the widely used methods to reduce the H_2S concentration, is considered for the BOXS-CC process.

$$ZnO_{(s)} + H_2S_{(g)} \longrightarrow ZnS_{(s)} + H_2O_{(g)} \quad \text{(R1)}$$

The purified syngas is then pressurised to 300 bar for combustion (Figure 1). The rest of the O_2 stream produced in the ASU, which comprises the stoichiometric amount of O_2 required for syngas combustion and 5% excess O_2 to ensure complete combustion, is heated to 200°C before being sent to the first combustion stage. To prevent the excessive temperature in the combustor, the combustion products from the first stage along with the unreacted O_2 are fed to the second combustion stage, where they are acting as a coolant. This process continues until the syngas is entirely consumed in the last combustion stage. Moreover, further cooling at each combustion stage occurs as heat is extracted to pre-heat the CO_2 stream in the supercritical CO_2 (sCO_2) cycle. The exhaust gas is then cooled down by transferring heat for pre-heating the oxygen streams and district heating. The water vapour in the cold exhaust gas is condensed and separated. The remaining stream that contains high purity CO_2 is sent to the CO_2 purification unit (CPU) to be conditioned for storage (Figure 1). In the sCO_2 cycle, as shown in Figure 1, the CO_2 stream is pressurised to 300 bar by pump and compressor. Before entering the sCO_2 turbine, it is heated in a low-temperature recuperator (LTR) and high-temperature recuperator (HTR), as well as the multi-stage combustor.

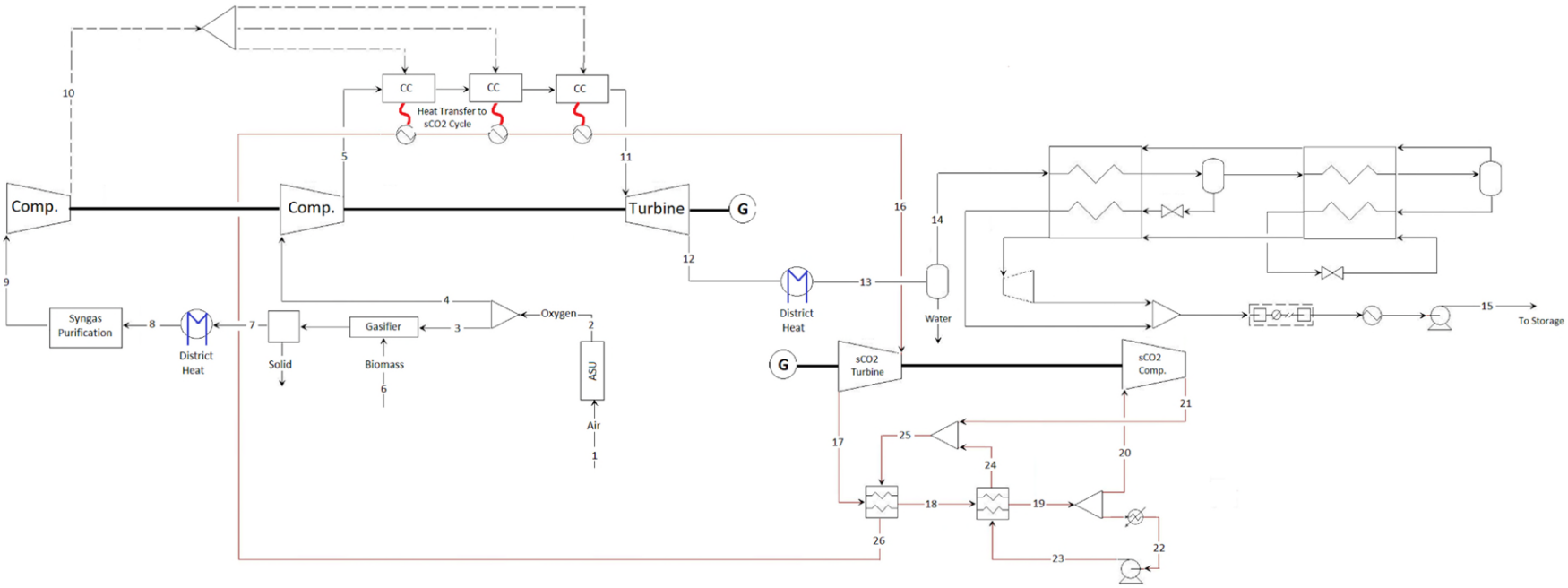

Figure 1. Simplified process flow diagram of BOXS-CC cycle.

2.1. Model development

The process model for the BOXS-CC process was developed in Aspen Plus®. The equation of state used for thermodynamic property estimation was the Peng Robinson. The biomass and solid residues were defined as the non-conventional components. Biomass enters the yield reactor, which was simulated by using the *RYIELD* block where decomposition occurs to form conventional components such as C, H_2, O_2, H_2O, N_2 and S. Thereafter, components from decomposition along with O_2 entered the gasifier block. The heat required for decomposition was supplied through partial oxidation with the sub-stoichiometric amount of oxygen supplied. The gasifier and all combustion chambers were simulated using the Gibbs reactor (*RGibbs*), which utilises the principle of Gibbs energy minimisation to reach the equilibrium composition under specified conditions [23]. The gasification temperature was set at 750°C [24] by adjusting the O_2 flow rate to the gasifier. The *SSPLIT* block was used after the gasifier for the separation of solid residues from gas. The *Sep* unit was used for the syngas purification. The temperature and pressure of all combustion stages were set at 950°C and 300 bar, respectively. The *MHeatX* block was used with the minimum temperature approach of 5°C to represent the recuperators in the sCO_2 cycle [25,26]. All other heat exchangers, including heater and cooler, were modelled using the *Heater* block. The *Compr* block was used for all turbines and single-stage compressors. The water separator was modelled using *Flash2* block. The stream after condensation was sent to the CPU and then pressurised to 110 bar. The sCO_2 turbine inlet temperature was set at 700°C by implementing the design specification that adjusted the CO_2 mass flow rate in the sCO_2 cycle to arrive at the desired temperature. A cryogenic ASU was simulated using a standard double-column cryogenic unit with the high- and low-pressure columns operated at 5.6 and 1.3 bar, respectively, and filled with 350Y structured packing [27]. The O_2 purity in the ASU was set at 95%, associated with the minimum energy consumption for a cryogenic ASU [28]. It was assumed that cooling water at 15°C is available at the plant site and that heat losses are negligible. The properties of the biomass feedstock are presented in Table 1. Moreover, the key assumptions used to model the turbomachinery and the initial operating parameters for the BOXS-CC are presented in Table 2 and Table 3, respectively.

Table 1. Biomass feedstock composition

Parameter	Value
Biomass composition (wood flour) [29]	
Moisture (wt%, wet)	4.9
Carbon (wt%, dry)	47.0
Hydrogen (wt%, dry)	6.9
Nitrogen (wt%, dry)	3.4
Oxygen (wt%, dry)	42.2
Sulphur (wt%, dry)	0.1
Ash (wt%, dry)	0.4
Proximate analysis	
Volatile matter (wt%, dry)	77.3
Fixed carbon (wt%, dry)	17.7
Ash (wt%, dry)	0.4
Lower heating value (MJ/kg)	15.3

Table 2. Turbomachinery design conditions

Parameter	Value
Isentropic efficiency of pump (%) [30]	90
Isentropic efficiency of the turbine (%) [30]	93
Isentropic efficiency of the compressor (%) [30]	89
Mechanical efficiency of compressors and pump (%) [31]	99.6
Electrical efficiency of the generator (%)[32]	98.5
Combustor and gasifier pressure drop (mbar)	150
Pressure drop in heat exchangers (%)	1

Table 3. Initial BOXS-CC operating parameters

Parameter	Value
Combustor pressure (bar)	300
Combustor temperature (°C)	950
Gasifier temperature (°C)	750
Turbine backpressure (bar)	35
sCO_2 turbine inlet temperature (°C)	700
sCO_2 turbine inlet pressure (bar)	300
sCO_2 turbine backpressure (bar)	75
Recompression split fraction (-)	0.2

2.2. Model validation

The considered BOXS-CC process consists of a syngas gasification section and two power generation sections: (1) the staged oxy-combustion power cycle and (2) the sCO_2 cycle. The power generation sections have been previously validated and investigated extensively by Khallaghi et al. [19,21]. The accuracy of the gasification model used in this study is validated based on the wood chip oxy-gasification reported by Dimitriou et al. [33]. The prediction of the model developed in this study was in good agreement with the literature data, Table 4.

Table 4. Benchmark of the syngas composition

Component (vol%)	Dimitriou et al. [33]	This study
H_2O	12.6	12.2
H_2	28.3	28.5
CO	26	26.4
CO_2	21.2	22.2
CH_4	10.5	10.3
N_2	0.56	0.39
H_2S	0.02	0.01

3. Technical assessment

To evaluate the thermodynamic performance of the BOXES-CC, the net power efficiency (η_{net}), heat efficiency (η_{heat}) and total efficiency (η_{total}) of the considered system are defined in Eqs. (1), (2) and (3), respectively. The net power output ($\boldsymbol{\dot{W}_{net}}$) is calculated as the gross power output less the system's parasitic load. The amount of heat available for district heating ($\boldsymbol{Q_{heat}}$) calculated as the sum of the heat from cooling the syngas and exhaust gas streams. The chemical energy input is defined as the product of the fuel consumption rate ($\dot{m}_{fuel}$) and the lower heating value (LHV).

$$\eta_{net} = \frac{W_{net}}{\dot{m}_{fuel} \cdot LHV} \tag{1}$$

$$\eta_{heat} = \frac{Q_{heat}}{\dot{m}_{fuel} \cdot LHV} \tag{2}$$

$$\boldsymbol{\eta_{total} = \eta_{net} + \eta_{heat}} \tag{3}$$

3.1. Thermodynamic performance

Table 5 presents the thermodynamic assessment based on the initial input parameters from Tables 1-3. It reveals that this concept has a net power output of 283.5 MW and the heat output of 211 MW available for district heating. Such output corresponded to net power and heat efficiencies of 36.9% and 27.4%, respectively, leading to the total efficiency of 64.3%. It can be seen that the sCO_2 compression imposes the main parasitic load on the system, as it accounts for more than 22% of the total thermal energy input in the system.

Table 5. Performance summary of BOXS-CC based on initial operating parameters

Component	Value
Thermal energy input (MW)	768.3
High-pressure turbine (topping cycle) (MW)	60.3
sCO_2 turbine power output (MW)	559.2
Air separation unit power consumption (MW)	56.9
O_2 compression power consumption (MW)	35.8
Syngas compression (MW)	74.8
sCO_2 compression stage power consumption (MW)	173.8
CO_2 compression power consumption (MW)	4.7
Net power output (MW)	283.5
Net electric efficiency (%)	36.9
Heat output (MW)	211.0
Heat efficiency (%)	27.4
Total efficiency (%)	64.3

To improve the performance of the BOXS-CC system, a sensitivity analysis was performed on the split fraction ($\boldsymbol{SF}$) in the sCO_2 cycle, gasification temperature and combustion temperature. It is worth noting that the effects of the pressure and temperature in the sCO_2 cycle have been extensively analysed in the literature [19,21]. Therefore, the sensitivity analysis of these parameters is not included in the scope of this work. It needs to be emphasised that when a single recuperator is used in the sCO_2 cycle, a pinch problem occurs due to an imbalance in the specific heat of the sCO_2 streams [25]. This is due to a large variation in the specific heat of CO_2 with temperature and pressure, especially in the vicinity of the critical point [34]. To compensate for this imbalance, the sCO_2 stream is split after the low-temperature recuperator. The diverted CO_2 stream is recompressed without heat rejection before merging the main CO_2 stream between both recuperators, as shown in Figure 1. This split is characterised by the SF defined as the fraction of the total CO_2 flow entering the high-temperature recuperator.

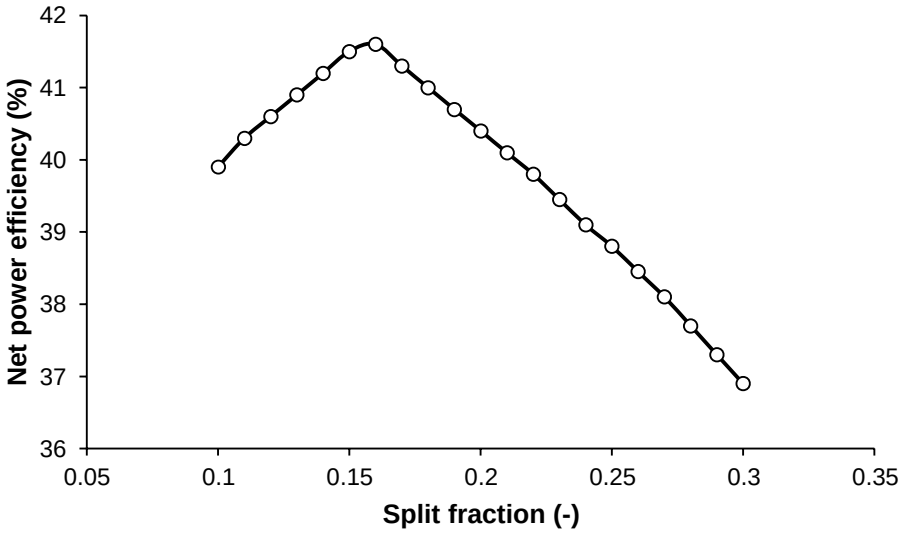

Figure 2. Effect of the split fraction on the net electric efficiency

Analysis of the effect of SF on the thermodynamic performance (Figure 2) has revealed that the value of 0.16 would result in the highest net power efficiency of 41.6%. This is because, at this SF rate, the approach temperature is minimised at both ends of the low-temperature recuperator, maximising the heat transfer rate. Moreover, Figure *3* represents the effect of the gasification temperature on the BOXS-CC performance. The gasification temperature was adjusted by controlling the O_2 mass flow rate, while other parameters, such as the sCO_2 turbine inlet temperature (700°C) and the combustion temperature (950°C) were kept constant. The results revealed an increase in the gasification temperature from 750°C to 900°C, resulting in an increase in the heat efficiency from 27.4% to 28.8%. This was because more heat is available for district heating (Figure 4). On the one hand, the net electric efficiency decreased from 41.6% to 40.1%. This can be explained by the fact that more heat from the syngas stream before compression is transferred to district heating. This balances the drop in the net power output. As a result, the total efficiency of the cycle remained around 69%.

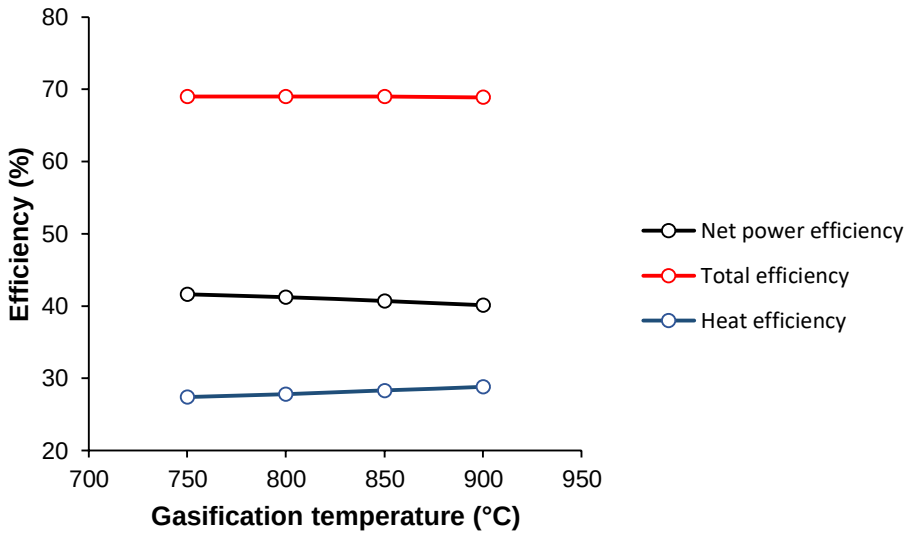

Figure 3. Effect of gasification temperature on the cycle performance

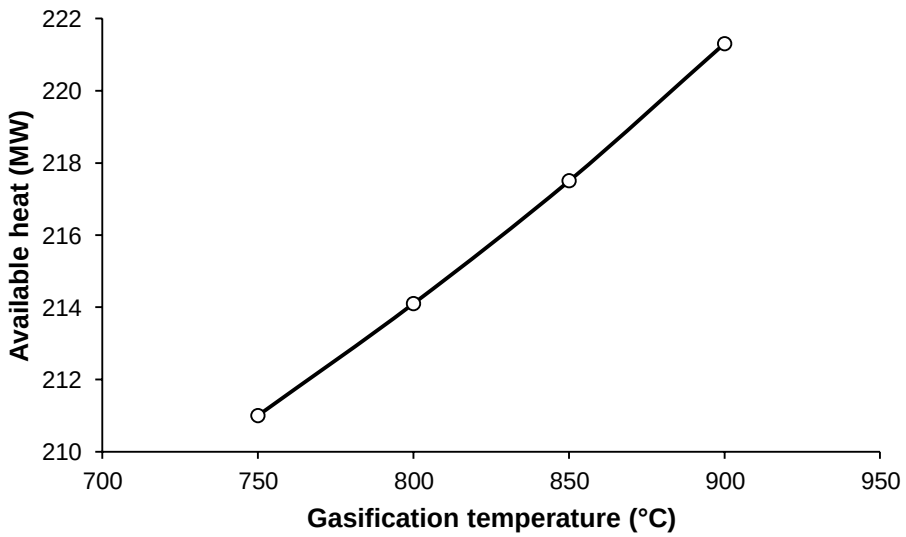

Figure 4. Effect of gasification temperature on heat available for district heating

Furthermore, Figure 5 showed the effect of the combustion temperature on the BOXS-CC performance at the gasification temperature of 750°C. It can be seen that although the net power efficiency drops from 41.6% at 950°C to 39.5% at 1150°C, the total efficiency increases from 69.0% to 70.3%. This was a result of less heat being transferred to the sCO_2 cycle at each combustion stage at higher combustion temperatures. Therefore, to keep the sCO_2 turbine inlet temperature at 700°C, the CO_2 mass flow rate reduced, leading to the subsequent reduction in the power output of the sCO_2 turbine by 6.2% (35 MW) (Figure 6). On the contrary, due to a higher inlet

temperature, the power output of the high-pressure turbine was increased by 17.2% (10.4 MW). This figure was less than the drop in the power output of the sCO_2 turbine, leading to a reduction in the net power efficiency. Nevertheless, an increase in the high-pressure turbine inlet temperature resulted in more heat for district heating (Figure 7), increasing the total efficiency.

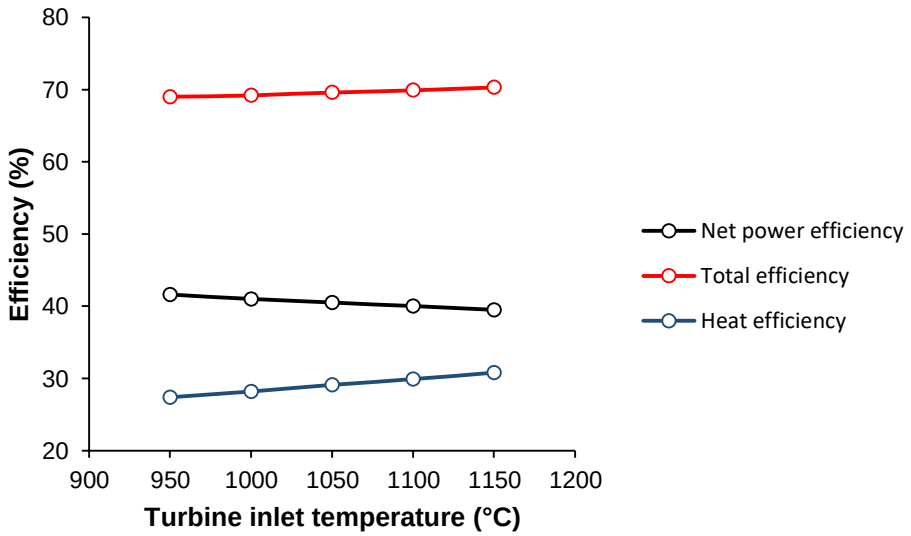

Figure 5. Effect of the combustion temperature on the BOXS-CC performance

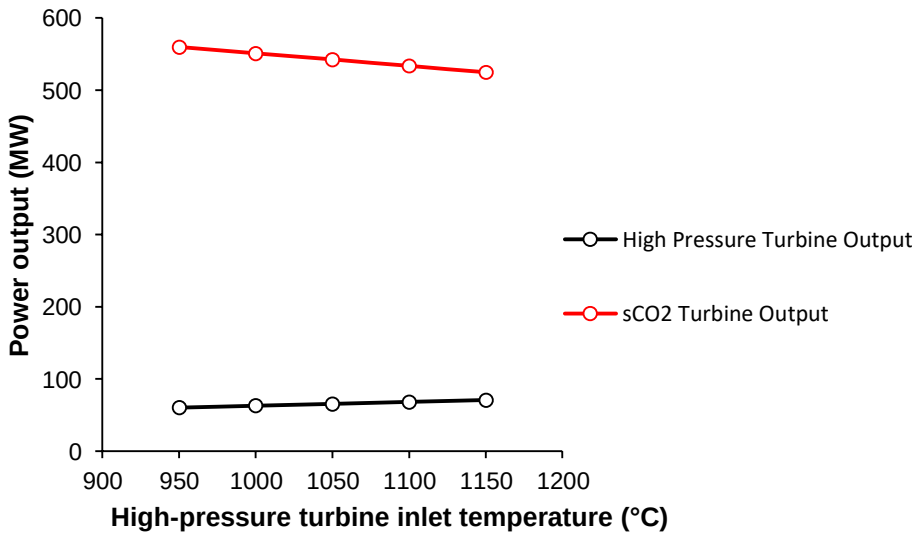

Figure 6. Effect of the combustion temperature on power output

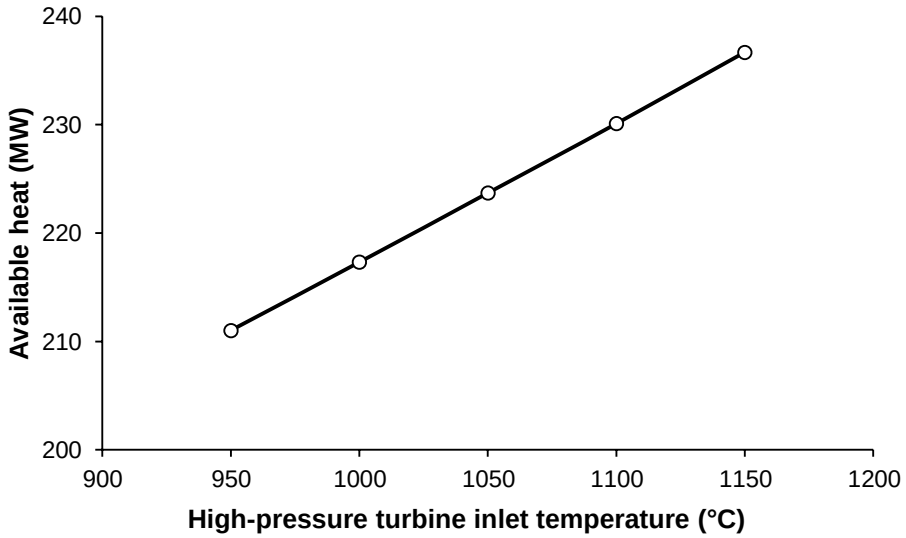

Figure 7. Effect of the combustion temperature on heat available for district heating

However, it needs to be highlighted that without EGR being used to lower the combustion temperature in the BOXS-CC, working under high temperature (1150°C) is intolerable. Moreover, the results indicated that the difference in the total efficiency between 950°C and 1150°C at 300 bar is only 1.3%. Therefore, the thermodynamic performance of the BOXS-CC under 300 bar and 950°C is summarised in Table 6. The analysis shows that the proposed concept has a net power output of 319.6 MW with net power and total efficiencies of 41.6% and 69.0%, respectively.

Table 6.Thermodynamic performance of BOXS-CC based on revised operating parameters

Component	Value
Thermal energy input (MW)	768.3
High-pressure turbine (topping cycle) (MW)	60.3
sCO_2 turbine power output (MW)	559.6
Air separation unit power consumption (MW)	56.9
O_2 compression power consumption (MW)	25.8
Syngas compression (MW)	74.8
sCO_2 compression stage power consumption (MW)	138.3
CO_2 purification and compression power consumption (MW)	4.5
Net power output (MW)	319.6
Net power efficiency (%)	41.6
Heat output (MW)	211.0
Heat efficiency (%)	27.4
Total efficiency (%)	69.0

Compared to the state-of-the-art NGCC with a net efficiency above 62% [35] and an NGCC with CO_2 capture, which results in a net efficiency penalty of more than 8% [36], the BOXS-CC is characterised by a lower net power efficiency (41.6%). However, the lower power efficiency of the BOXS-CC is compensated by the generation of heat for district heating, which results in a total efficiency of 69.0%.

4. Economic assessment

The economic evaluation of the BOXS-CC was performed using the levelised cost of electricity ($\boldsymbol{LCOE}$), Eq. (4). To do so, the total annualised cost ($\boldsymbol{TAC}$) that comprise the annualised total plant cost ($\boldsymbol{TPC}$), the fuel cost ($\boldsymbol{FC}$), the carbon revenue ($\boldsymbol{C_{carbon}}$), variable ($\boldsymbol{V_{O\&M}}$) and fixed ($\boldsymbol{F_{O\&M}}$) operating and maintenance costs, Eq. (5).

$$LCOE = \frac{TAC}{8760 \times W_{net} \times CF} \tag{4}$$

$$TAC\left[\frac{M€}{y}\right] = TPC \times FCF + FC + C_{Carbon} + V_{O\&M} + F_{O\&M} \tag{5}$$

$\boldsymbol{TPC}$ equals the sum of direct capital cost (purchase cost), indirect capital cost. Indirect Capital Cost (ICC) comprises project contingency and the owner's cost. The annualised TPC equals the TPC multiply by the fixed charge factor ($\boldsymbol{FCF}$), which is defined using Eq. (6), considering the project interest rate (r) and project lifetime (T).

$$\boldsymbol{FCF = \frac{r(1+r)\,T}{(1+r)\,T-1}} \tag{6}$$

1. The assumptions used in the economic analysis are summarised in Table 7.

Table 7. Assumptions for the economic analysis

Parameter	Value
Indirect capital cost ($\boldsymbol{ICC}$) as a fraction of total purchase cost (%) [37]	45
Variable operating cost ($\boldsymbol{VOM}$) as a fraction of total capital cost (%) [31]	2.0
Fixed operating cost ($\boldsymbol{FOM}$) as a fraction of total capital cost (%) [31]	1.0
Wood flour price (€/t_{dry}) [38]	68.5
Plant lifetime ($\boldsymbol{T}$) (years) [31]	25
Project interest rate ($\boldsymbol{r}$) (%) [31]	8.75

The equipment purchase costs ($\boldsymbol{C_B}$) for gasifier, sulphur removal, CPU, gas turbine, heat exchanger and compressor were calculated based on reference cost data from the literature (Table 8) using Eq. (7) where $\boldsymbol{C_A}$ is the cost of the reference component with the capacity of $\boldsymbol{Q_A}$ and $\boldsymbol{f}$ is the scaling factor. It is worth noting that although a simple separator is considered for the BOXES-CC modelling, an entire sulphur removal plant with a recovery section is considered for the cost analysis.

$$C_B = C_A \left(\frac{Q_B}{Q_A}\right)^f \tag{7}$$

Table 8. Scaling parameters for the component purchase cost

Component	Scaling factor	C_A (M€)	Q_A	f	Ref.
Gasification reactor	Mass flow (t/h)	48.53	54.4	0.75	[11]
Sulphur removal and recovery	Mass flow (t/h)	43.33	452.6	0.67	[39]
CPU	Mass flow (t/h)	55.98	266.6	0.6	[40]
Compressor	Power (kW)	0.44	413	0.68	[40]
Gas turbine	Power (MW)	49.4	272.1	0.3	[41]
Heat exchanger	Heat transfer (MW)	6.1	828	0.67	[42]

The correlations used to estimate the capital costs of other components are summarised in Table 9. The following correlations relate the purchasing cost of each component ($\boldsymbol{C_i}$), to their operating parameters such as mass flow rate ($\boldsymbol{m_i}$), pressure ratio ($\boldsymbol{\beta}$), isentropic efficiency ($\boldsymbol{\eta_i}$), turbine inlet temperature ($\boldsymbol{T_T}$).

Table 9. Capital cost estimation correlation

Equipment [scaling parameter]	Correlation
sCO_2 Turbine [mass flow at the inlet to the turbine $\boldsymbol{m_T}$ (kg/s), Isentropic efficiency $\boldsymbol{\eta_T}$(-), Pressure ratio $\boldsymbol{\beta}$(-), Turbine inlet temperature $\boldsymbol{T_{T,i}}$ (C)] [43]	$\boldsymbol{C_{Turbine} = \dot{m}_T \cdot \beta \cdot \left(\frac{392.2}{1-\eta_T}\right) \cdot ln(\beta)\left(1 + \exp\left(0.036\, T_{T,i} - 65.66\right)\right)}$
Air separation unit [O_2 production rate, $\boldsymbol{m_{O2}}$(kg/s)] [44]	$\boldsymbol{C_{ASU} = 2.926 e^{7} \left(\frac{m_{O2}}{28.9}\right)^{0.7}}$
Generator [Break power output, $\boldsymbol{W_{T,BRK}}$(kW) [45]	$\boldsymbol{C_{Gen} = 26.18\ (W_{T,BRK})^{0.95}}$

4.1. Economic performance

The economic feasibility of the proposed concept was evaluated by considering the LCOE at different heat and carbon trading prices. The breakdown of the capital cost for the considered case is shown in Table 10. The total plant cost of the BOXS-CC was estimated to be €585.4M. It has been shown that the gasifier has the highest contribution to the total capital cost.

Table 10. Economic performance of the BOXS-CC

	Unit	Value
ASU	M€	54.9
CPU	M€	59.3
Gasification reactor	M€	119
Gas turbine	M€	28.8
sCO_2 turbine	M€	37.8
Compressors	M€	24.2
Generators	M€	6.9
Heat exchangers	M€	30.5
Total equipment cost	M€	391.6
Total plant cost (TPC)	M€	585.4
Annualised TPC	M€/y	52.8
Fuel cost	M€/y	86.4
Fixed O&M	M€/y	5.8
Variable O&M	M€/y	11.7
Total annualised cost	M€/y	156.7
LCOE	€/MWh	70

Table 10 reveals that when there is no revenue from negative CO_2 emission, the LCOE (€70/MWh) is higher than the electricity prices reported for fossil fuel power plants without CO_2 capture (€32.5/MWh–€63.8/MWh) [31]. However, Figure 8 shows that the LCOE of the BOXS-CC was highly sensitive to changes in the carbon price. At the carbon price of €40/tCO_2, the LCOE is around €33/MWh, which is in the range of the conventional NG-fuelled power cycles without CO_2 capture. Considering the carbon price of €120/tCO_2 in some European countries such as Sweden in 2017 [46], the carbon price of €40/tCO_2 is reasonable.

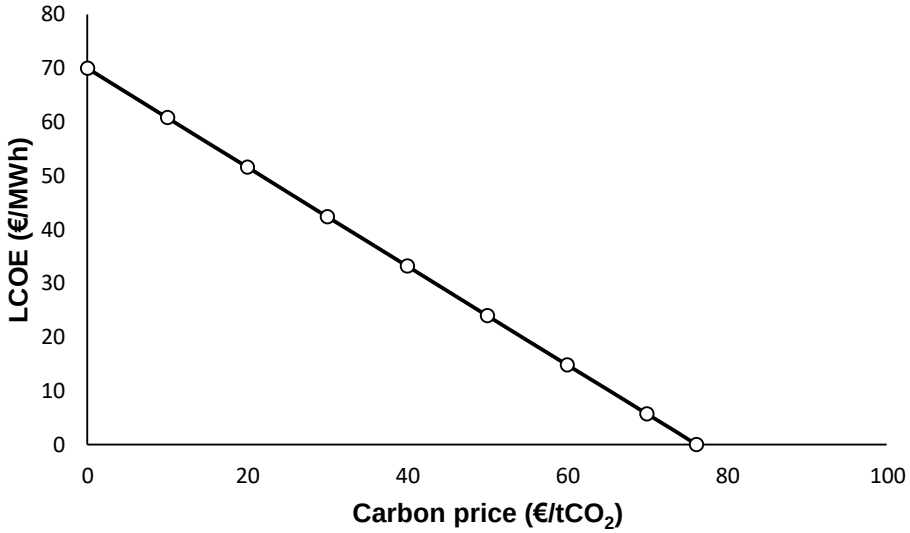

Figure 8. Effect of the carbon price on the economic performance of the BOXS-CC

The effect of the heat price on the LCOE at different values of the carbon price is presented in Figure 9. Moreover, some technical constraints such as energy resource availability or economic reasons may result in different capacity factor. Therefore, the effect of a different capacity factor on the LCOE is presented in Figure 10 while the heat and carbon prices are kept at €46.5/MWh [47] and €40/tCO_2, respectively.

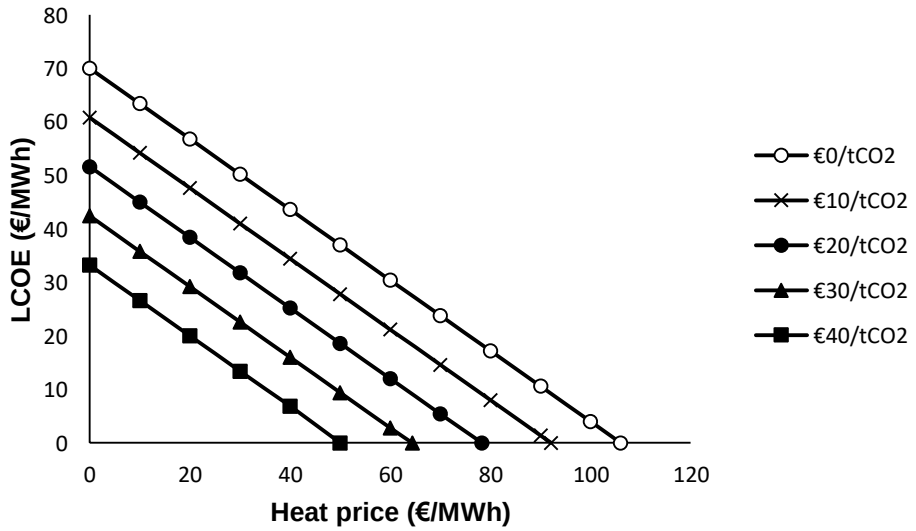

Figure 9. Effect of heat price on the economic performance of the BOXS-CC.

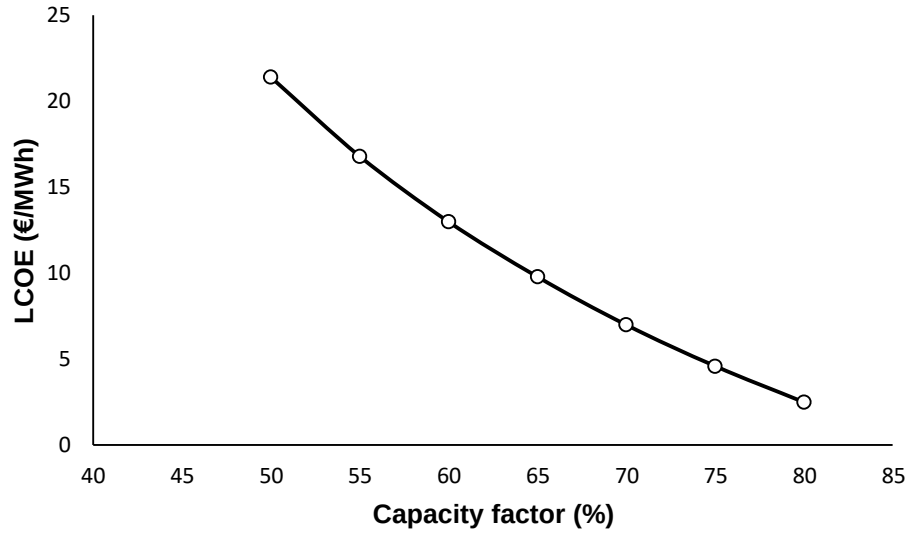

Figure 10. Effect of the capacity factor on the economic performance of the BOXS-CC

It has been shown that the economic performance of the BOXS-CC is susceptible to changes in both heat price (Figure 9) and capacity factor (Figure 10). Figure 10 reveals that at a capacity factor of 50%, the LCOE would be €21.4/MWh. This LCOE is superior to other fossil fuel power plants with CO_2 capture plants (€45/MWh-€90.5/MWh) [31]. Therefore, further development of the BOXS-CC would contribute to the decarbonisation of the power sector, and even negative emissions can be achieved at an affordable cost.

5. Environmental assessment

The environmental assessment focuses on quantifying the net greenhouse gas (GHG) emissions associated with BOXS-CC system. The assessment has been carried out following the life cycle assessment (LCA) methodology as per the ISO 14040 [48] and 14044 standards [49]. The global warming potential (GWP) impact is estimated as per IPCC -AR5 [50]. The plant is assumed to be situated in the UK. The scope of the study is from the production of feedstock to the compression of CO_2 ready for storage. The system boundary includes the construction of the BOXS-CC plant, production of sawdust, its transport, production of electricity and heat in BOXS-CC plant, treatment of H_2S, and carbon capture for storage. It is assumed that the feedstock (sawdust) for the BOXS plant is imported from Canada. Ash and ZnS waste are assumed to be landfilled. The functional unit is defined as the ‘generation of 1 MWh of electricity’.

Table 11 provides a summary of input and output data for the system. The background LCA data for the feedstock, equipment, transport, waste disposal and other relevant processes have been sourced from Ecoinvent v3.7 [51]. The GHG impact of manufacturing the plant components (i.e. gasifier, gas turbine, and compressor) has been estimated by upscaling the Ecoinvent data using the scaling factor (f) in Table 8. Since the plant also provides heat as a co-product, exergy allocation has been used to allocate the impact between electricity and heat.

Table 11. Life cycle inventory data for the BOXS-CC system

Data	Value
Feedstock ($\boldsymbol{kg/MWh_e}$)	658
Sea transport (Canada to the UK) ($\boldsymbol{t.km/MWh_e}$)	4260
Road transport (Canada) ($\boldsymbol{t.km/MWh_e}$)	132
Road transport (UK) ($\boldsymbol{t.km/MWh_e}$)	132
Catalyst (ZnO) ($\boldsymbol{kg/MWh_e}$)	0.4
Waste (ash and catalyst) ($\boldsymbol{kg/MWh_e}$)	3.1
Wastewater (ash and catalyst) ($\boldsymbol{m^3/MWh_e}$)	0.3
Heat (co-product) ($\boldsymbol{MWh_{th}/MWh_e}$)	0.66
Exergy allocation factor (heat) (%)	10
CO_2 captured (before allocation for heat) ($\boldsymbol{kg/MWh_e}$)	921

5.1. Environmental performance

As shown in Figure 11, the BOXS-CC system results in net negative emissions of 766 kg CO_2 eq./MWh_e. The background emissions associated with the supply chain and the plant components are estimated at 62.5 kg CO_2 eq./MWh_e. The main contributor to the background GHG emissions is transporting, which contributes 90%, followed by the production of feedstock and other inputs, which accounts for 8%. The contributions of plant construction and waste treatment and disposal are very small.

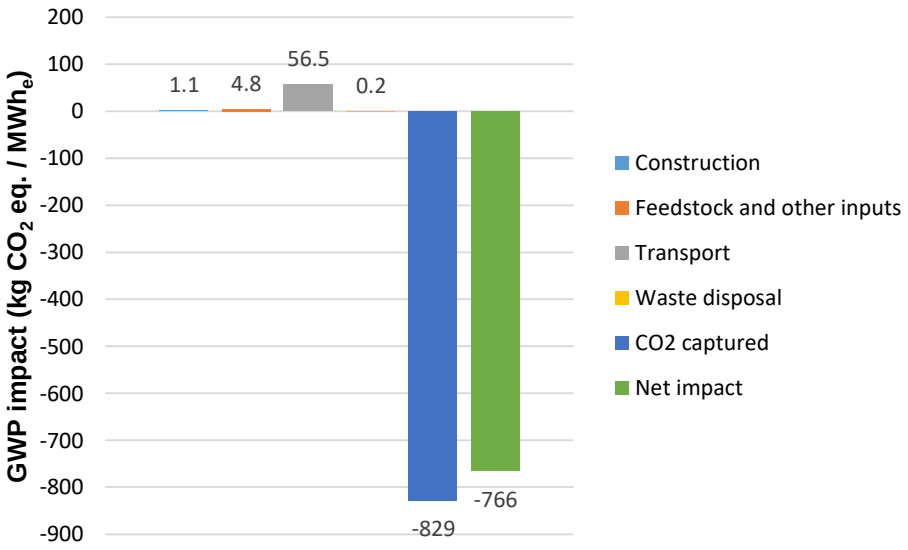

Figure 11. Greenhouse gas emission for generation of 1 MWh of electricity from the BOXS-CC (after 10% allocation for heat)

6. Conclusions

This study presented a CO_2-negative emission concept of biomass oxy-gasification integrated with the combined heat and power system based on staged syngas oxy-combustion combined cycle (BOXS-CC). The techno-economic feasibility analysis revealed that the integration of staged-combustion concept with biomass gasification has the potential to compensate the energy penalty associate with biomass oxy-gasification. The results revealed that the proposed cycle was characterised with net power efficiency and total efficiency of 41.6% % and 69.0%, respectively. The economic assessment revealed that at the capacity factor of 50%, the levelised cost of electricity (LCOE) was €21.4/MWh, considering a heat price of €46.5/MWh and carbon price of €40/tCO_2. Such economic performance was competitive compared to fossil fuel power plants with and without CO_2 capture. The environmental assessment shows that BOX-CC system results in net negative emissions of 766 kg CO_2 eq./MWh_e. Overall, the BOXS-CC was shown to have the potential to contribute to significant cost reduction in decarbonising the power and heat sector while achieving negative CO_2 emissions to offset the CO_2 emissions from other sources.

List of Abbreviations

BOXS-CC	Biomass oxy-gasification staged combustion combined cycle
CCS	Carbon capture and storage

BECCS	Bio-energy with carbon capture and storage
CHP	Combined heat and power
NG	Natural gas
SOF-NGCC	Staged oxy-fuel natural gas combined cycle
ASU	Air separation unit
NGCC	Natural gas combined cycle
LTR	Low-temperature recuperator
HTR	High-temperature recuperator
sCO_2	Supercritical CO_2
CPU	Carbon purification unit
LHV	Lower heating value
TIT	Turbine inlet temperature
LCOE	Levelised cost of electricity
SOFC	Solid oxide fuel cell

Nomenclature

A_{HE}	Heat exchanger surface area [m^2]
C_j	Capital cost of equipment j [£]
CF	Capacity factor [-]
FCF	Fixed charge factor [-]
FOM	Fixed operating and maintenance cost [£]
k	Correction coefficient
LCOE	Levelised cost of electricity [£/MWh]
LHV	Lower heating value [kJ/kg]
$\dot{m}_{fuel}$	Fuel consumption rate [kg/s]
$\dot{m}_{O_2}$	O_2 production rate in air separation unit [kg/s]
SFC	Specific fuel cost [£/MWh]
TCR	Total capital requirement [£]
T_{T_i}	Turbine inlet temperature [°C]
VOM	Variable operating and maintenance cost [£/MWh]
$\dot{W}_{j,BRK}$	Break power output/requirement of equipment j [MW]
W_{net}	Net power output of the entire system [MW]
η_{heat}	Heat efficiency
η_j	Isentropic efficiency of equipment j [%]
η_{net}	Net efficiency [%]
η_{total}	Total efficiency
β	Pressure ratio [-]

References

[1] GEA. Global Energy Assessment-Toward a Sustainable Future. Cambridge University Press, Cambridge UK and New York, NY, USA and the International Institute for Applied Systems Analysis, Laxenburg, Austria: 2012.

[2] Bui M, Adjiman CS, Anthony EJ, Boston A, Brown S, Fennell PS, et al. Carbon capture and storage (CCS): the way forward. Energy Environ Sci

2018;11:1062–176. https://doi.org/10.1039/c7ee02342a.

[3] CCC. Meeting Carbon Budgets: Closing the policy gap. 2017.

[4] Global CCS institute. Global status of CCS 2017. Dockland, Australia: 2017.

[5] Department of Energy & Climate Change. CCS Roadmap: Supporting deployment of Carbon Capture and Storage in the UK. 2012.

[6] Fajardy M, Chiquier S, Mac Dowell N. Investigating the BECCS resource nexus : delivering sustainable negative emissions. Energy Environ Sci Sci 2018;11:3408–30. https://doi.org/10.1039/c8ee01676c.

[7] Pour N, Webley PA, Cook PJ. Opportunities for application of BECCS in the Australian power sector. Appl Energy 2018;224:615–35. https://doi.org/10.1016/j.apenergy.2018.04.117.

[8] Withey P, Johnston C, Guo J. Quantifying the global warming potential of carbon dioxide emissions from bioenergy with carbon capture and storage. Renew Sustain Energy Rev 2019;115:109408. https://doi.org/10.1016/j.rser.2019.109408.

[9] Situmorang YA, Zhao Z, Yoshida A, Abudula A, Guan G. Small-scale biomass gasification systems for power generation (< 200 kW class): A review. Renew Sustain Energy Rev 2020;117:109486. https://doi.org/http://doi.org/10.1016/j.rser.2019.109486.

[10] Dinca C, Slavu N, Cormos C-C, Badea A. CO_2 capture from syngas generated by a biomass gasi fi cation power plant with chemical absorption process. Energy 2018;149:925–36. https://doi.org/10.1016/j.energy.2018.02.109.

[11] Zang G, Jia J, Tejasvi S, Ratner A, Silva Lora E. Techno-economic comparative analysis of Biomass Integrated Gasification Combined Cycles with and without CO_2 capture. Int J Greenh Gas Control 2018;78:73–84. https://doi.org/10.1016/j.ijggc.2018.07.023.

[12] Xiang Y, Cai L, Guan Y, Liu W, He T, Li J. Study on the biomass-based integrated gasification combined cycle with negative CO_2 emissions under different temperatures and pressures. Energy 2019;179:571–80.

https://doi.org/10.1016/j.energy.2019.05.011.

[13] Franco A, Bellina F. Methods for optimized design and management of CHP systems for district heating networks (DHN). Energy Convers Manag 2018;172:21–31. https://doi.org/10.1016/j.enconman.2018.07.009.

[14] Jang Y, Lee J. Optimizations of the organic Rankine cycle-based domestic CHP using biomass fuel. Energy Convers Manag 2018;160:31–47. https://doi.org/10.1016/j.enconman.2018.01.025.

[15] Perna A, Minutillo M, Cicconardi SP, Jannelli E, Scarfogliero S. Conventional and advanced biomass gasification power plants designed for cogeneration purpose. Energy Procedia 2015;82:687–94. https://doi.org/10.1016/j.egypro.2015.11.793.

[16] Pérez NP, Machin EB, Pedroso DT, Roberts JJ, Antunes JS, Silveira JL. Biomass gasification for combined heat and power generation in the Cuban context: Energetic and economic analysis. Appl Therm Eng 2015;90:1–12. https://doi.org/10.1016/j.applthermaleng.2015.06.095.

[17] Ruiz JA, Juárez MC, Morales MP, Muñoz P, Mendívil MA. Biomass gasification for electricity generation: Review of current technology barriers. Renew Sustain Energy Rev 2013;18:174–83. https://doi.org/10.1016/j.rser.2012.10.021.

[18] Khallaghi N, Hanak DP, Manovic V. Techno-economic evaluation of near-zero CO_2 emission gas-fired power generation technologies: A review. J Nat Gas Sci Eng 2020;74:103095. https://doi.org/10.1016/j.jngse.2019.103095.

[19] Khallaghi N, Hanak DP, Manovic V. Staged oxy-fuel natural gas combined cycle. Appl Therm Eng 2019;153:761–7. https://doi.org/10.1016/j.applthermaleng.2019.03.033.

[20] Mancuso L, Ferrari N, Chiesa P, Martelli E, Romano M. Oxy-combustion turbine power plants. n.d.

[21] Khallaghi N, Hanak DP, Manovic V. Gas-fired chemical looping combustion with supercritical CO_2 cycle. Appl Energy 2019;249:237–44. https://doi.org/10.1016/j.apenergy.2019.04.096.

[22] Zhang W, Liu H, Ul Hai I, Neubauer Y, Schröder P, Oldenburg H, et al. Gas cleaning strategies for biomass gasification product gas. Int J Low-Carbon Technol 2012;7:69–74. https://doi.org/10.1093/ijlct/ctr046.

[23] Khan MN, Shamim T. Investigation of hydrogen generation in a three reactor chemical looping reforming process. Appl Energy 2016;162:1186–94. https://doi.org/10.1016/j.apenergy.2015.08.033.

[24] Pala LPR, Wang Q, Kolb G, Hessel V. Steam gasification of biomass with subsequent syngas adjustment using shift reaction for syngas production : An Aspen Plus model. Renew Energy 2017;101:484–92. https://doi.org/10.1016/j.renene.2016.08.069.

[25] Padilla RV, Soo Too YC, Benito R, Stein W. Exergetic analysis of supercritical CO_2 Brayton cycles integrated with solar central receivers. Appl Energy 2015;148:348–65. https://doi.org/10.1016/j.apenergy.2015.03.090.

[26] Turchi CS, Ma Z, Neises T, Wagner M. Thermodynamic Study of Advanced Supercritical Carbon Dioxide Power Cycles for High Performance Concentrating Solar Power Systems. ASME 2012 6th Int Conf Energy Sustain Parts A B 2012;135:375. https://doi.org/10.1115/ES2012-91179.

[27] Hanak DP, Powell D, Manovic V. Techno-economic analysis of oxy-combustion coal-fired power plant with cryogenic oxygen storage. Appl Energy 2017;191:193–203. https://doi.org/10.1016/j.apenergy.2017.01.049.

[28] Soundararajan R, Gundersen T, Ditaranto M. Oxy-combustion coal based power plants : Study of operating pressure , oxygen purity and downstream purification parameters. Chem Eng Trans 2014;39:229–34. https://doi.org/10.3303/CET1439039.

[29] Lan W, Chen G, Zhu X, Wang X, Liu C, Xu B. Biomass gasification-gas turbine combustion for power generation system model based on ASPEN PLUS. Sci Total Environ 2018;628–629:1278–86. https://doi.org/10.1016/j.scitotenv.2018.02.159.

[30] Santini L, Accornero C, Cioncolini A. On the adoption of carbon dioxide thermodynamic cycles for nuclear power conversion: A case study applied to

Mochovce 3 Nuclear Power Plant. Appl Energy 2016;181:446–63. https://doi.org/10.1016/j.apenergy.2016.08.046.

[31] Hanak DP, Jenkins BG, Kruger T, Manovic V. High-efficiency negative-carbon emission power generation from integrated solid-oxide fuel cell and calciner. Appl Energy 2017;205:1189–201. https://doi.org/10.1016/j.apenergy.2017.08.090.

[32] Hanak DP, Manovic V. Economic feasibility of calcium looping under uncertainty. Appl Energy 2017;208:691–702. https://doi.org/10.1016/j.apenergy.2017.09.078.

[33] Dimitriou I, Goldingay H, Bridgwater A V. Techno-economic and uncertainty analysis of Biomass to Liquid (BTL) systems for transport fuel production. Renew Sustain Energy Rev 2018;88:160–75. https://doi.org/10.1016/j.rser.2018.02.023.

[34] Ahn Y, Bae SJ, Kim M, Cho SK, Baik S, Lee JI, et al. Review of supercritical CO_2 power cycle technology and current status of research and development. Nucl Eng Technol 2015;47:647–61. https://doi.org/10.1016/j.net.2015.06.009.

[35] Smith RW. Steam turbine cycles and cycle design optimization: combined cycle power plants. Adv. Steam Turbines Mod. Power Plants, 2017, p. 57–92.

[36] Sanchez Fernandez E, Goetheer ELV, Manzolini G, Macchi E, Rezvani S, Vlugt TJH. Thermodynamic assessment of amine based CO_2 capture technologies in power plants based on European Benchmarking Task Force methodology. Fuel 2014;129:318–29. https://doi.org/10.1016/j.apenergy.2014.04.066.

[37] Al Lagtah NMA, Onaizi SA, Albadarin AB, Ghaith FA, Nour MI. Techno-economic analysis of the effects of heat integration and different carbon capture technologies on the performance of coal-based IGCC power plants. J Environ Chem Eng 2019;7:103471. https://doi.org/10.1016/j.jece.2019.103471.

[38] Emenike O, Michailos S, Finney KN, Hughes KJ, Ingham D, Pourkashanian M. Initial techno-economic screening of BECCS technologies in power generation for a range of biomass feedstock. Sustain Energy Technol Assessments

2020;40:100743. https://doi.org/10.1016/j.seta.2020.100743.

[39] Dagie R, Li XS, Spies K, Rainbolt J, Braunberger B, King D, et al. Coal-Derived Warm Syngas Purification and CO_2 Capture- Assisted Methane Production. 2014.

[40] Cormos AM, Dumbrava I, Cormos CC. Evaluation of techno-economic performance for decarbonized hydrogen and power generation based on glycerol thermo-chemical looping cycles. Appl Therm Eng 2020;179:115728. https://doi.org/10.1016/j.applthermaleng.2020.115728.

[41] Gazzani M, Turi DM, Manzolini G. Techno-economic assessment of hydrogen selective membranes for CO_2 capture in integrated gasification combined cycle. Int J Greenh Gas Control 2014;20:293–309. https://doi.org/10.1016/j.ijggc.2013.11.006.

[42] Manzolini G, Giuffrida A, Cobden PD, van Dijk HAJ, Ruggeri F, Consonni F. Techno-economic assessment of SEWGS technology when applied to integrated steel-plant for CO_2 emission mitigation. Int J Greenh Gas Control 2020;94:102935. https://doi.org/10.1016/j.ijggc.2019.102935.

[43] Michalski S, Hanak DP, Manovic V. Techno-economic feasibility assessment of calcium looping combustion using commercial technology appraisal tools Techno-economic feasibility assessment of calcium looping combustion using commercial technology appraisal tools. J Clean Prod 2019;219:540–51. https://doi.org/10.1016/j.jclepro.2019.02.049.

[44] Atsonios K, Koumanakos A, Panopoulos KD, Doukelis A, Kakaras E. Techno-economic comparison of CO_2 capture technologies employed with natural gas derived GTCC. Proc. ASME Turbo Expo, San Antonio, Texas, USA: 2013.

[45] Aminyavari M, Haghighat Maghami A, Shirazi A, Najafi B, Rinaldi F. Exergetic, economic, and environmental evaluations and multi-objective optimization of an internal-reforming SOFC-gas turbine cycle coupled with a Rankine cycle. Appl Therm Eng 2016;108:833–46. https://doi.org/10.1016/j.applthermaleng.2016.07.180.

[46] Haites E. Carbon taxes and greenhouse gas emissions trading systems: what

have we learned? Clim Policy 2018;18:955–66. https://doi.org/10.1080/14693062.2018.1492897.

[47] Yang Y, Wang J, Chong K, Bridgwater A V. A techno-economic analysis of energy recovery from organic fraction of municipal solid waste (MSW) by an integrated intermediate pyrolysis and combined heat and power (CHP) plant. Energy Convers Manag 2018;174:406–16. https://doi.org/10.1016/j.enconman.2018.08.033.

[48] ISO. Environmental Management - Life Cycle Assessment - Principles and Framework (ISO 14040:2006). Geneva, Switzerland: 2006.

[49] ISO. ISO 14044: Environmental Management - Life cycle assessment - Requirements and guidelines. Geneva, Switzerland: 2006.

[50] Myhre, G. D, Shindell F-M, Bréon W, Collins J, Fuglestvedt J, Huang D, et al. Anthropogenic and Natural Radiative Forcing. In: Climate Change 2013: The Physical Science Basis. Contribution of Working Group I to the Fifth Assessment Report of the Intergovernmental Panel on Climate Change. Cambridge, United Kingdom and New York, NY, USA: 2013.

[51] Ecoinvent. Ecoinvent v3.7 database. Dübendorf, Switzerland: Swiss Centre for Life Cycle Inventories: 2020.